








Cite this: *Org. Chem. Front.*, 2019, **6**, 3374

Optimization of the synthesis of quinoline-based neutral cyclometalated iridium complexes *via* microwave irradiation: design of light harvesting and emitting complexes using bulky quinolines†

Carlos A. Echeverry-Gonzalez, ^a Carlos E. Puerto-Galvis, ^a Carlos H. Borca, ^b Martín A. Mosquera, ^c Andrés F. Luis-Robles^a and Vladimir V. Kouznetsov ^{*a}

We report an optimized synthesis of neutral heteroleptic cyclometalated iridium complexes based on bidentate ligands (C[^]N) of 2-phenylpyridine and 2-phenylquinoline derivatives and an ancillary ligand (L[^]X) of acetylacetonone *via* microwave (MW) irradiation. The developed methodology increases yields up to 85% with significantly lower reaction times and solvent consumption in comparison with conventional heating. The robustness of our methodology is demonstrated through the high-yield synthesis of bulky 2-phenylquinoline derivatives leading to three new complexes, which show desirable optical properties with absorption tails extending up to 650 nm and relative quantum yields of up to 0.210. In addition, the spin-allowed transitions for these complexes exhibit solvatochromism and are, therefore, characterized experimentally and computationally.

Received 8th July 2019,
Accepted 21st August 2019
DOI: 10.1039/c9qo00870e
rsc.li/frontiers-organic

Introduction

In the last two decades, organic and inorganic–organic compounds for optoelectronic applications have received increasing attention due, mainly, to their optical properties which can be easily tuned through synthetic design. These compounds have been widely applied in photovoltaics,^{1,2} artificial photosynthesis,^{3,4} sensors,^{5–7} and phosphorescent organic light emitting diodes (PhOLEDs).⁸ Noteworthy, among these compounds, neutral cyclometalated iridium complexes also have been widely applied in these fields.^{9–11} However, the applications of these complexes in visual displays and lighting technologies have been the most studied to date^{12–14} because of (i) high photoluminescent quantum yields by strong spin orbit coupling, (ii) simple emission color tuning by changes in the electron density of the main ligands due to large ligand field splitting, and (iii) high thermo- and photostability.^{15–17} Likewise, in recent years, the study of cyclo-

metalated iridium complexes has also been extended to the field of photovoltaics.^{18,19}

Different types of iridium complexes have been reported in the literature. These complexes can be classified as homoleptic and heteroleptic depending on the nature of the surrounding bidentate ligand. Homoleptic iridium complexes have three equal bidentate ligands (C[^]N), whereas heteroleptic complexes have two equivalent C[^]N ligands and an ancillary ligand commonly named the L[^]X ligand. Given the variety of combinations of C[^]N and L[^]X ligands, the properties of heteroleptic iridium complexes have been studied more broadly than those of homoleptic iridium complexes.^{20,21}

Since the original work by Forrest and co-workers in 2000,²² the synthesis of heteroleptic cyclometalated iridium(III) complexes has focused on the use of novel ligands with promising photophysical, electrochemical, and electrophosphorescent properties.^{23,24} Among them, complexes based on quinoline derivatives exhibited high external quantum efficiencies (EQEs) ranging from 10% to 30% with β -diketones,^{25,26} 2-phenylpyridines,²⁷ oxadiazoles,²⁸ pyrazolyl-pyridines,²⁹ and phosphorus–sulfur (P = S) derivatives as ancillary ligands.³⁰

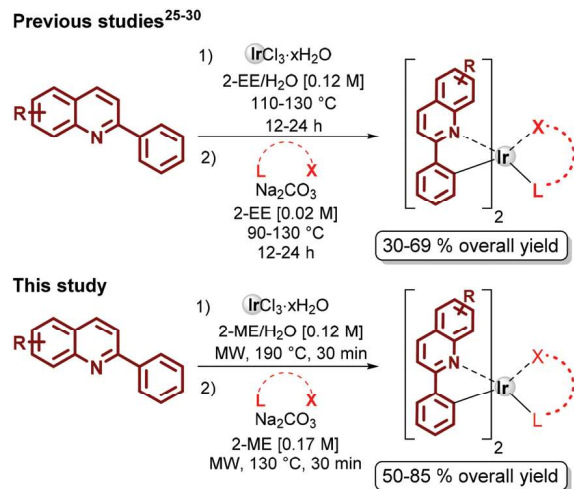
However, the current protocols for the synthesis of iridium(III) complexes cyclometalated by quinoline ligands are still time- and energy-consuming. Each step of this transformation often takes more than 12 hours at temperatures above 130 °C under conventional heating and demands excessive use of solvent, limiting the efficiency of the whole process.^{25–30} Lacking a greener, milder, and efficient alternative suitable for

^aLaboratorio de Química Orgánica y Biomolecular, CMN, Universidad Industrial de Santander, Parque Tecnológico Guatigará, Km 2 vía refugio, Piedecuesta, A.A. 681011, Colombia. E-mail: kouznet@uis.edu.co

^bSchool of Chemistry and Biochemistry, Georgia Institute of Technology, 901 Atlantic Drive NW, Atlanta, Georgia, 30332, USA

^cDepartment of Chemistry, Northwestern University, 2145 Sheridan Road, Evanston, Illinois 60208, USA

†Electronic supplementary information (ESI) available. See DOI: 10.1039/c9qo00870e



Scheme 1 Synthesis of heteroleptic cyclometalated Ir(III) complexes based on quinoline ligands.

the synthesis of valuable iridium(III) complexes, we found motivation to study how this reaction could be assisted by microwave (MW) irradiation. This would enable higher reaction temperatures, increased reaction yields, reduced reaction times, and enhanced reproducibility and robustness (Scheme 1).^{31,32} Although there has been interest in using MW irradiation to synthesize iridium(III) compounds,^{33,34} the reported approaches are mainly focused on the synthesis of neutral homoleptic or cationic heteroleptic complexes, with a reaction time of 80 min at 200 °C, yielding moderate to high yields.³⁵ However, to the best of our knowledge, reported procedures for the synthesis of neutral heteroleptic cyclometalated iridium(III) complexes omitted the used MW irradiation.

In this study we report (i) the optimal reaction conditions for the first MW irradiation-driven synthesis of neutral heteroleptic cyclometalated iridium(III) complexes, (ii) the synthesis of iridium(III) complexes based on different quinoline (C[^]N) and ancillary ligands (L[^]X) under the optimized reaction conditions, and (iii) the photophysical and computational characterization of the new neutral cyclometalated iridium(III) complexes.

Results and discussion

The synthesis of neutral heteroleptic iridium complexes with ancillary ligands involves two consecutive steps. First, the iridium salt, usually IrCl_3 , reacts with two equivalents of the C[^]N ligand to provide the chloride-bridged dimer $[(\text{C}^{\wedge}\text{N})_2\text{IrCl}]_2$. Subsequently, the dimer reacts with the ancillary ligand L[^]X in the presence of a base to give the heteroleptic cyclometalated iridium(III) complex $[\text{C}^{\wedge}\text{N}]_2\text{Ir}[\text{L}^{\wedge}\text{X}]$. The reaction of the C[^]N ligands with iridium(III) halides requires drastic conditions, requiring a polar solvent with a high boiling point, usually 2-methoxy or 2-ethoxyethanol.³⁶ Thus, we selected 2-phenylpyridine (**1a**, C[^]N ligand) and acetylacetonate (**3a**, L[^]X ligand) as model substrates, and followed previously reported

reaction conditions under conventional heating^{14,22} to obtain the chloride-bridged dimer $[(2\text{-PhPy})_2\text{IrCl}]_2$, **2a**. This reaction achieved nearly quantitative yield from **1a** after 24 h at 120 °C using a mixture of 2-methoxyethanol (2-ME) and water as a solvent system in a 3 : 1 ratio (20 mL). Then, the intermediate **2a** was subjected to a Na_2CO_3 treatment with the ancillary ligand **3a** for 6 h at 80 °C using 2-ME as the solvent (20 mL), resulting in the desired iridium(III) complex $(2\text{-PhPy})_2\text{Ir}(\text{acac})$ **4a** with a 43% yield (Table 1, entry 1).

In our first attempt to improve the reaction conditions under MW irradiation, we estimated the temperature and time according to the Arrhenius equation, using the parameters described in entry 1 for the global process (Table 1).³⁷ Thus, performing the first step at 190 °C for 30 min under microwave irradiation using 2-ME and water as a solvent system (1.4 mL), we isolated the chloride-bridged dimer **2a** at quantitative yield, after washing and centrifuging (4000 rpm) with diethyl ether. Then, for the second step, only 0.5 mL of 2-ME was used as the solvent. After 30 min of MW irradiation at 130 °C, we obtained complex **4a** with a yield of 83% after column chromatography (Table 1, entry 2).

Other methodologies for synthesizing ionic iridium complexes have used solvents with different heating factor quotients ($\tan \delta$) such as ethyleneglycol^{33,35} and tetrahydrofuran.³⁸ It is also known that using acetonitrile as the solvent under conventional heating might interfere with the synthesis of complexes with acac as the ancillary ligand.^{39,40} Therefore, we studied the solvent effect on this reaction. Each solvent in Table 1 was irradiated with increasing temperature to reach 190 °C or a pressure ranging from 15 to 20 bar (see Fig. S1A in the Experimental section in the ESI[†]).

Although we isolated the dimer **2a** at a good yield when ethylene glycol was used as the solvent in the first step, the second step resulted in several decomposition byproducts by TLC, see Fig. S1B in the ESI[†] (Table 1, entry 3). Therefore, ethylene glycol was replaced by 2-ME in the second step, to evaluate the influence of the chosen reaction media in the first step. In this case, complex **4a** was isolated with a slight increase in the yield up to 59% in comparison with conventional heating (Table 1, entries 1 and 4). The washing procedures required to isolate dimer **2a** suggest that higher purity is achieved by TLC when ethylene glycol is used in the first step than that achieved when 2-ME is employed. However, the green solid obtained with ethylene glycol in this step suggests the presence of unreacted IrCl_3 as previously described by Monos *et al.* (Fig. S1B[†])³⁵ Likewise, the protic nature of ethylene glycol undermines the complexation of the metal center with the ancillary ligand. Tetrahydrofuran and acetonitrile were also tested but they dramatically lowered the reaction yields in both steps, resulting in the desired product with yields of 5 and 31%, respectively (Table 1, entries 5 and 6). Nevertheless, when 2-ME was employed in step 1 and acetonitrile in step 2, we isolated **4a** with a yield of 44% (Table 1, entry 7). To demonstrate that our protocol is robust and versatile, even with different ancillary ligands, we synthesized complex **4ab** using metformin (**3b**) as the L[^]X ligand with high yield (85%, Table 1, entry 8).

Table 1 Optimization of reaction conditions for the synthesis of neutral heteroleptic iridium complexes (2-PhPy)₂Ir(acac) **4a** and (2-PhPy)₂Ir(metformin) **4ab** under microwave irradiation

Entry	Complex	Step 1 ^a			Step 2 ^b			Overall yield ^c , %	
		Solvent, [M]	Temperature, °C	Time, min	L^X	Solvent, [M]	Temperature, °C		Time, min
1	4a	2-ME/H ₂ O [0.12]	120	24 h	3a	2-ME [0.02]	80	6 h	43
2		2-ME/H ₂ O [0.16]	190	30		2-ME [0.37]	130	30	83
3		Ethylene glycol/H ₂ O [0.16]	190	30		Ethylene glycol [0.37]	130	30	NR ^d
4		Ethylene glycol/H ₂ O [0.16]	190	30		2-ME [0.37]	130	30	59
5		THF/H ₂ O [0.16]	190	30		THF [0.37]	130	30	5
6		CH ₃ CN/H ₂ O [0.16]	190	30		CH ₃ CN [0.37]	130	30	31
7		2-ME/H ₂ O	190	30		CH ₃ CN [0.37]	130	30	44
8	4ab	2-ME/H ₂ O [0.16]	190	30	3b	2-ME [0.37]	130	30	85

^a Step 1: **1** (57.2 mg, 0.37 mmol), IrCl₃·xH₂O (50 mg, 0.17 mmol), and solvent system (ratio 3 : 1), temperature, time, MW irradiation was performed on a Biotage® Initiator + operating at a frequency of 2450 MHz, a high power of 4, and 18–20 bar. ^b Step 2: **2** (1 equiv.), **3** (6 equiv.), sodium carbonate (15 equiv.) and solvent (6 mL equiv.⁻¹), temperature, time, MW irradiation was performed on a Biotage® Initiator + operating at a frequency of 2450 MHz, a high power of 4, and 4–5 bar. ^c Isolated yield after column chromatography (SiO₂). ^d NR: no reaction.

Table 2 Substrate scope during the synthesis of heteroleptic cyclometalated iridium(III) complexes **4b–j** under MW irradiation^a

Complex	Yield (%)
4b	65%
4c	53%
4d	63%
4e	50%
4f	67%
4g	71%
4h	72%
4i	73%
4j	NR ^c

^a Step 1: **1b–j** (0.37 mmol), IrCl₃·xH₂O (50 mg, 0.17 mmol), and 2-ME : H₂O (1.4 mL, ratio 3 : 1), 190 °C, 30 min, MW irradiation was performed on a Biotage® Initiator + operating at a frequency of 2450 MHz, a high power of 4, and 18–20 bar. Step 2: **2b–i** (1 equiv.), **3a** (6 equiv.), sodium carbonate (15 equiv.) and 2-ME (6 mL), 130 °C, 30 min, MW irradiation was performed on a Biotage® Initiator + operating at a frequency of 2450 MHz, a high power of 4, and 4–5 bar. ^b Isolated yield after column chromatography (SiO₂). ^c NR: no reaction.

After optimizing the reaction conditions, we proceeded to evaluate the substrate scope of this reaction using simple to complex 2-phenyl quinolines as C^N ligands (Table 2). These

quinoline derivatives were synthesized with moderate to excellent yields, using the Povarov reaction as previously reported (see the ESI, Table S1†). In general, the respective dimers **2b–j**

derived from 2-phenyl quinolines **1b–j** were obtained in good to excellent yields (>82%) in all cases. However, a significant decrease in the reaction yields of step 2 was observed and complexes **4b–e** were obtained with yields of 50–65%, whereas the iridium derivatives of bulky C^N ligands **4f–i** were obtained with higher yields, despite the steric hindrance of the quinoline ligands substituted with the 1-naphthyl group at C-2 **1f** (67%), the diphenylamine moiety at C-6 **1g** (71%), and the 2-naphthyl group at C-2 **1h** (72%) and **1i** (73%) (Table 2). Unfortunately, in the case of ligand **1j**, where the quinoline core was substituted with a thiophene ring at C-2, the corresponding dimer **2j** could not be isolated. This is because, under the reaction conditions (MW irradiation for 30 min at 190 and 170 °C), the substrate decomposed into a complex mixture (Table 2). The structural identities of **4a–i** were fully established by ¹H and ¹³C NMR, as well as mass spectrometry (MALDI-TOF).

Photophysical properties

The absorption and emission spectra of the new complexes **4g–i** are shown in Fig. 1, and their data are summarized in Table 3. Absorption and emission were recorded in dichloromethane in all cases. Coordination to iridium led to intense absorption bands with ϵ values ranging from 3000 to 94 100 M⁻¹ cm⁻¹ and absorption tails, in some complexes,

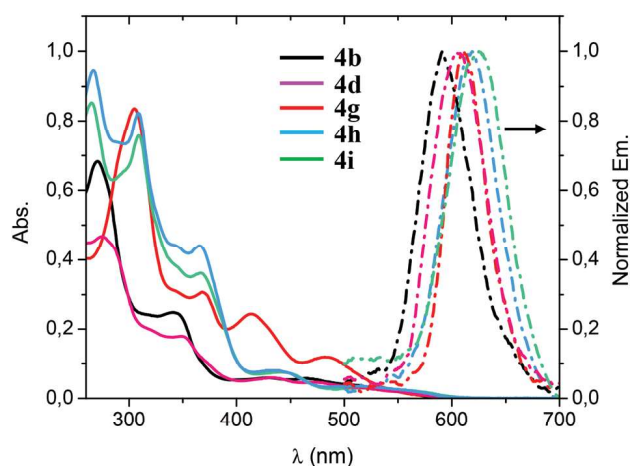


Fig. 1 Absorption and normalized emission spectra of the reference complexes **4b** and **4d**, and the new complexes **4g–i** recorded in dichloromethane at a concentration of 1.0×10^{-5} M at 298 K.

extending up to 650 nm. According to previous studies on cyclometalated complexes, the intense bands presented up to 400 nm can be attributed to spin-allowed ligand-centered transitions (¹ π to π^*) that are generally centered on quinoline ligands, while broad bands at lower energy can be attributed to both metal-to-ligand charge transfer (¹MLCT) and ligand-to-ligand charge transfer (¹LLCT) transitions.⁴¹ As shown in Table 3, the new complexes showed higher absorption than the reference complexes **4b** and **4d** for which absorption tails were extended only up to 600 nm. The presence of diphenylamine at the 6-position of the quinoline ring in **4g** notably changed the absorption features in comparison with **4b**. It led to a redshift of the most intense bands (*ca.*, 30 nm) and to the rise of two new bands at 414 and 482 nm with the ϵ values of 24 400 and 12 000 M⁻¹ cm⁻¹, respectively, improving the light harvesting properties of **4g**. The incorporation of the naphthyl group into **4h** and **4i** also improved the ϵ values in a wide range of the spectrum, which were higher than those of their homologous **4d** (Table 3), which is evidenced by the transition bands around 440 nm, with absorption tails extending up to 650 nm. This observation could be possibly attributed to spin-forbidden charge-transfer transitions, due to the strong spin-coupling associated with iridium.

The absorption spectra were recorded using different solvents for complexes **4g–i** (Fig. S12, ESI[†]) and their data are summarized in Table S2 (ESI[†]). Complexes **4g–i** showed the highest absorptions in dichloromethane and the lowest ones in acetonitrile for almost all transitions, except for the low energy transitions that were higher in toluene. Among the empirical correlations of the absorption band positions for complexes **4g–i**, we explore a measure of the ionizing power of the solvents E_T (Reichardt–Dimroth solvent functions) (ESI 2.4.1.†). The relationship between the position of the absorption bands in cm⁻¹ with E_T was determined using Pearson's r coefficients, and the linear fits are shown in Fig. S13A–D for **4g** (ESI[†]).

For MLCT and LLCT transitions (>400 nm), a correlation can be seen between the solvent shifts of absorption band positions and E_T , showing an r -coefficient of 0.93 and 0.98. Also, the transition bands were hypsochromically shifted as the E_T of the solvents increased (Fig. S13A and B[†]). Interestingly, π to π^* transitions (<400 nm) were also shifted, bathochromically when toluene and dimethylformamide were used and hypsochromically in the case of dichloromethane and acetonitrile. It is thought that the position of the absorp-

Table 3 Photophysical characteristics of the iridium complexes

Complex	$\lambda_{\text{max}}^{\text{abs}}/\text{nm}$ (ϵ , M ⁻¹ cm ⁻¹)	$\lambda_{\text{max}}^{\text{em}}/\text{nm}$	Stokes' shift/cm ⁻¹	E_{0-0}/eV	Φ_{PL}^b
4b ^a	271(68 000), 343(25 000)	591	12 234	3.62	0.301
4d ^a	275(46 400), 350(18 100)	604	12 015	2.85	0.260
4g	305(83 600), 369(30 800), 414(24 400), 482(12 000)	611	4295	2.56	0.210
4h	309(82 100), 367(44 100), 439(8700), 508(3100)	620	3556	2.44	0.135
4i	309(75 900), 366(36 300), 446(7700), 520(3000)	626	3073	2.36	0.103

^a These complexes were used as reference. ^b Emission quantum yield relative to [Ru(bpy)₃](PF₆)₂ ($\Phi = 0.062$ in MeCN) as standard.⁴²

tion bands of the spin-allowed π - π^* ligand-centred transitions is independent of E_T . This is mainly due to the lack of strong changes in the dipole moments upon electronic excitation, as seen for CT transitions. These π to π^* transitions proved to be solvent sensitive as the MLCT and LLCT transitions.

The normalized emission spectra of complexes **4g-i** at an excitation wavelength of 420 nm in dichloromethane featured a single band bathochromically shifted with the increase of the conjugation (e.g., the presence of diphenylamine in **4g** shifted at 20 nm the $\lambda_{\text{max}}^{\text{em}}$ in comparison with **4b**, Fig. 1). The inclusion of the fluorine substituent in **4i** shifted by 6 nm the $\lambda_{\text{max}}^{\text{em}}$ in comparison with **4h** having a methyl substituent at the 6-position of the quinoline ring (Table 3). To determine whether the emission spectra were independent of the excitation wavelength, emissions were recorded by wavelength sweep.

Relative quantum yields (Φ_{PL}) were measured in dichloromethane with an excitation wavelength of 420 nm using $[\text{Ru}(\text{bpy})_3](\text{PF}_6)_2$ ($\Phi = 0.062$ in acetonitrile) as standard.⁴² The reference complexes **4b** and **4d** showed higher Φ_{PL} than the new complexes **4g-i**, and amongst the latter ones, **4g** showed the highest Φ_{PL} of 0.210 (Table 3). Interestingly, the presence of the methyl group in complex **4h** increased Φ_{PL} in comparison with **4i**. The trend of the Φ_{PL} values agrees with the calculated E_{0-0} values showing that the lower the gap between the ground and excited states, the less efficient the radiative process.⁴³ It is important to mention that although complexes **4g-i** showed lower Φ_{PL} values than the reference complexes, these Φ_{PL} values are comparable with those of emitting complexes used in optoelectronic devices previously reported.^{34,44}

Quantum chemical calculations

To further elucidate the optical properties of the synthesized iridium complexes, Density Functional Theory (DFT) calcu-

lations were performed for **4g-i**. These calculations were performed in two stages: a geometry optimization and a linear-response time-dependent (TD) calculation. The optimized geometry structures, the highest occupied and lowest unoccupied molecular orbital (HOMO and LUMO) energy values, and their spatial distributions for the complexes are compiled in Table S3 (ESI[†]).

The optimized structures show that these complexes are imperfect octahedra (Fig. S14, ESI[†]). For **4g**, the angle between the quinoline and the acac ligand is 113.2°, while the angles in **4h** and **4i** are slightly more acute (113.1° for both complexes). The $>20^\circ$ variation with respect to the perfect octahedral coordination environment exhibited by **4g-i** suggests that these complexes are structurally stressed mainly due to the small L^X ligand (acac). This increases the probability of detaching this ligand through a light-induced mechanism or by replacement with a different one.

The HOMOs for complexes **4g-i** are predominately located over the iridium atom, the L^X ligand (acac), and the naphthyl rings for the case of **4h** and **4i**. However, the LUMOs are distributed over segments of the quinoline ligand, probably due to their electron-deficient character (Fig. 2). As expected, the incorporation of electron-donating groups such as diphenylamine and methyl destabilizes the HOMO of **4g** and **4h**, as reflected by the HOMO energy values of $-4.2(5)$ eV and $-4.2(2)$ eV, respectively, compared to $4.4(9)$ eV in **4i**. By contrast, the fluorine substituent, at the 6-position of the quinoline ring, stabilizes the HOMO in **4i**. The presence of electron-donating substituents destabilizes the LUMOs, leading to an increase of HOMO-LUMO gap (E_{Gap}), whose values are close to the optical gaps (E_{0-0}) calculated from the experimental spectra (Table 3), indicating the good agreement of experimental and computational results. It is also worth noting that E_{Gap} becomes larger as the destabilization of the LUMOs grows (Fig. 2).

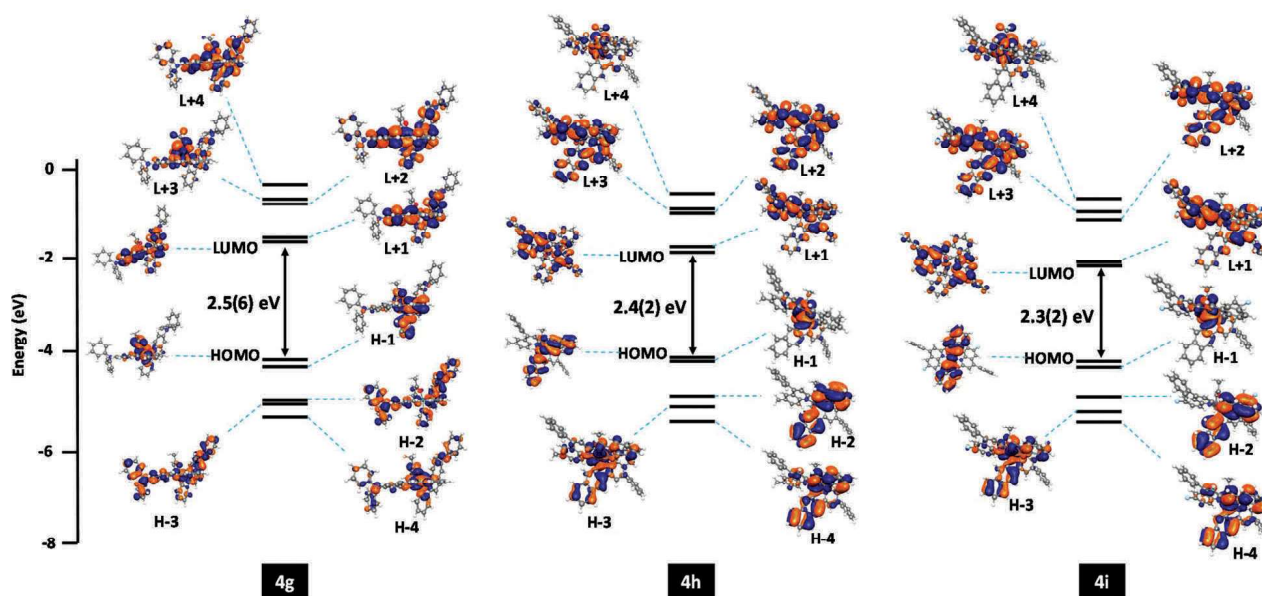


Fig. 2 Calculated energy-level scheme for orbitals ranging from HOMO-4 (H-4) to LUMO+4 (L+4) of complexes **4g-i**.

The LUMO stabilization gained by the incorporation of the fluorine group into **4i** results in a bathochromic shift of the most probable transitions, showing a low energy transition at 751 nm with an oscillator strength of 0.018. Transition-state calculations show high-energy absorption bands for all complexes between 250 and 300 nm attributed to spin-allowed $\pi\text{-}\pi^*$ ligand-centred (LC) transitions from the quinoline ligands. However, the absorption intensity drops off in the low energy region, which agrees with the experimental data (Fig. 1). The higher the oscillator strength for an electronic transition, the higher absorption coefficients the transitions will have, **4g** being the complex with the highest absorption coefficients in the low energy region.

Calculations indicate four different transitions >400 nm for **4g** with oscillator strengths ranging from 0.012 to 0.214, all contributing to the CT process (MLCT/LLCT/ILCT). For **4h** and **4i**, calculations predicted the largest shift of the low energy transitions toward the red region of the visible spectrum with energies of 1.72 and 1.65 eV, respectively. However, these complexes show weaker oscillator strengths than **4g** around this region. Fig. 2 shows the energies of the four highest-occupied and four lowest-unoccupied molecular orbitals for **4g-i**. For **4g**, HOMO-1 is just 0.1(2) eV more stable than HOMO and it is mainly localized over the iridium atom, acac and phenyl at the C-2 of the quinoline. In contrast, for **4h** and **4i**, HOMO-1 is distributed over the iridium atom and the acac ligands. For the case of HOMO-2 in **4g**, the orbital is distributed over the quinoline ligands with a large contribution of the diphenylamine substituents. However, for **4h** and **4i**, it is localized over both naphthyl groups. Finally, HOMO-3 and HOMO-4 are uniformly localized over the whole of the complexes.

The four lowest-unoccupied molecular orbitals for **4g-i** are mainly distributed over the quinoline ligands, except for L+3 of **4g** and L+4 of **4hg** and **4i**, which are localized over the acac ligand. The low energy transitions correspond to CT transitions, which are mainly described by H \rightarrow L, H-1 \rightarrow L, H-2 \rightarrow L, H \rightarrow L+1 and H-1 \rightarrow L+1 transitions (Table S3 \dagger).

Conclusions

Neutral heteroleptic cyclometalated iridium complexes with different C^N ligands were successfully synthesized in good to high yields using our MW methodology. This methodology demonstrated to be fast, simple, and robust, which is desirable for potential applications in optoelectronic devices. The use of 2-ME led to higher reaction yields in comparison with other solvents having different heating factor quotients ($\tan \delta$). Likewise, higher reaction yields were obtained when we used 2-PhPy ligands in comparison with 2-PhQu derivatives.

According to the emission measurements, complexes **4g-i** based on bulky-quinoline ligands showed shorter Stokes' shifts compared to **4b** and **4d**, thereby displaying lower E_{0-0} values, which resulted in lower Φ_{PL} . However, Φ_{PL} values were as high enough as those of red-emitting complexes reported in the literature. The photophysical and computational character-

ization studies of the new complexes provided important insights: (i) the coordination of bulky quinolines with electron donor substituents (*e.g.*, NPh₂ in **4g**) improves the light-harvesting ability, showing similar absorption features than photoactive complexes.^{45,46} For the case of complexes **4h-i**, absorption tails extending up to 650 nm due mainly to MLCT and ILCT transitions, as characterized through DFT calculations, decrease Φ_{PL} . Nonetheless, these absorption tails could be useful in optoelectronic applications, such as sensitizers in solar cells⁴⁶ and visible-to-UV photon upconversion,⁴⁷ where broader absorption properties are desired; and (ii) taking into consideration that the naphthyl groups in **4h** and **4i** have an important contribution to the HOMO topology, the introduction of electron-drawing substituents on these rings may improve Φ_{PL} .

Experimental section

General

The synthesis of neutral cyclometalated iridium complexes was performed using a Biotage® initiator Microwave Synthesizer. All reagents and solvents were used as purchased. All air-sensitive reactions were carried out under an argon atmosphere. Flash chromatography was performed using silica gel (Merck, Kieselgel 60, 230–240 mesh or Scharlau 60, 230–240 mesh). Analytical thin layer chromatography (TLC) was performed using aluminum coated Merck Kieselgel 60 F254 plates. NMR spectra were recorded on a Bruker Avance 400 (¹H: 400 MHz; ¹³C: 100 MHz) spectrometer at 298 K using partially deuterated solvents as internal standards. Coupling constants (*J*) are denoted in Hz and chemical shifts (δ) in ppm. Multiplicities are denoted as follows: s = singlet, d = doublet, t = triplet, m = multiplet, and br = broad. UV-Vis spectra were recorded on a Genesys 10 s spectrophotometer using toluene, chloroform, dichloromethane, dimethylformamide, acetonitrile and methanol as solvents. Emission spectra were recorded on a Photon Technology International spectrophotometer using dichloromethane and acetonitrile as solvents. MALDI experiments were carried out on a Bruker Ultraflex extreme MALDI TOF-TOF instrument (Bruker Daltonics, Billerica, MA) equipped with a 1 kHz Smart Beam Nd:YAG laser (355 nm), 6 ns pulse and a spot size of 100 μm —according to the manufacturer's specifications—using the FlexAnalysis software.

Computational methods and details

All DFT calculations on the new complexes were performed using the computational chemistry package NWChem version 6.6,⁴⁸ and the B3LYP functional with the 6-31G basis set for every element, except for iridium. The LANL08 basis set and its corresponding Effective Core Potential (ECP) were used for iridium. All computations were carried out using a fine grid for exchange–correlation integration. Linear-response TD-DFT calculations were performed on the optimized geometries of **4g-i**.

General synthetic procedure for neutral cyclometalated iridium complexes

The synthesis of neutral cyclometalated iridium complexes was performed in two steps *via* MW irradiation. Step 1: $\text{IrCl}_3 \cdot x\text{H}_2\text{O}$ (50 mg, 0.17 mmol), C^N ligand (57.2 mg, 0.37 mmol), and solvent: H_2O (1.4 mL) were irradiated by MW for 30 minutes (temperature: 190 °C; range of pressure: 18–20 bar; and high power). Then, the colored product (dimer) was centrifuged (15 min at 4000 rpm) and rinsed three times with diethyl ether to remove the unreacted quinoline derivative. Step 2: Dimer (1 eq.), acetylacetonone (6 eq.), sodium carbonate (15 eq.) and solvent (6 mL eq.⁻¹) were irradiated by MW for 30 minutes (temperature: 130 °C; range of pressure: 4–5 bar; and high power). Then, 2-methoxyethanol was evaporated to reduced pressure and the reaction crude was purified by SiO_2 chromatography using dichloromethane as the mobile phase.

Complex 4a. Yellow solid (83%, 84.6 mg). ¹H NMR (400 MHz, CDCl_3) δ : 8.50 (d, J = 5.8 Hz, 2H), 7.83 (d, J = 8.3 Hz, 2H), 7.71 (m, 2H), 7.53 (d, J = 8.0 Hz, 2H), 7.14–7.11 (m, 2H), 6.82–6.78 (m, 2H), 6.72–6.64 (m, 2H), 6.26 (d, J = 8.0 Hz, 2H), 5.21 (s, 1H), 1.78 (s, 6H) ppm. ¹³C-NMR (100 MHz, CDCl_3) δ : 184.6, 168.7, 148.2, 147.6, 144.7, 136.7, 133.1, 129.1, 123.8, 121.3, 120.7, 118.3, 100.3, 28.7 ppm. HRMS (MALDI): calcd for $\text{C}_{27}\text{H}_{23}\text{IrN}_2\text{O}_2$ 600.1389; found $[\text{M}^+] m/z$ 600.1392.

Complex 4ab. Yellow solid (85%, 91.0 mg). ¹H NMR (400 MHz, CDCl_3) δ : 8.69 (d, J = 4.0 Hz, 1H), 8.59 (d, J = 4.0 Hz, 1H), 7.83 (m, 5H), 7.55 (dd, J = 20.0, 8.0 Hz, 2H), 7.21 (br, 2H), 6.85–6.79 (m, 2H), 6.74–6.60 (m, 2H), 6.51 (br, 2H), 6.27–6.22 (m, 2H), 5.02 (s, 1H), 4.82 (s, 1H), 2.99 (s, 6H) ppm. ¹³C-NMR (100 MHz, CDCl_3) δ : 168.7, 168.7, 152.7, 152.6, 152.3, 149.0, 148.7, 144.6, 137.0, 132.7, 132.6, 129.6, 124.2, 124.1, 122.5, 121.3, 121.2, 118.9, 118.8, 39.8 ppm. HRMS (MALDI): calcd for $\text{C}_{26}\text{H}_{26}\text{IrN}_7$ 629.1879; found $[\text{M}^+] m/z$ 629.1877.

Complex 4b. Red solid (65%, 77.3 mg). ¹H NMR (400 MHz, CDCl_3) δ : 8.48 (d, J = 4.0 Hz, 1H), 8.17 (d, J = 8.0 Hz, 2H), 7.06 (d, 2H), 7.83–7.77 (m, 4H) 7.48–7.40 (m, 4H), 6.95–6.91 (m, 2H), 6.63–6.59 (m, 2H), 6.54–6.51 (m, 2H), 6.64 (s, 1H), 1.49 (s, 6H) ppm. ¹³C-NMR (100 MHz, CDCl_3) δ : 185.5, 170.4, 150.9, 149.3, 147.0, 138.0, 136.1, 130.4, 128.7, 127.7, 127.1, 126.7, 125.8, 120.9, 116.6, 116.5, 100.1, 28.2 ppm. HRMS (MALDI): calcd for $\text{C}_{35}\text{H}_{27}\text{IrN}_2\text{O}_2$ 700.1702; found $[\text{M}^+] m/z$ 700.1703.

Complex 4c. Red solid (53%, 79.0 mg). ¹H NMR (400 MHz, CDCl_3) δ : 8.48 (dd, J = 9.7, 5.2 Hz, 2H), 8.14–8.05 (m, 4H), 7.80 (dd, J = 7.8, 1.3 Hz, 2H), 7.42 (dd, J = 8.5, 2.9 Hz, 2H), 7.20–7.14 (m, 2H), 6.97–6.93 (m, 2H), 6.65–6.60 (m, 2H), 6.49 (dd, J = 6.0, 4.0 Hz, 2H), 4.67 (s, 1H), 1.50 (s, 6H) ppm. ¹³C-NMR (100 MHz, CDCl_3) δ : 185.7, 169.9, 150.3, 146.8, 146.2, 137.2, 137.2, 135.9, 129.3, 129.2, 128.8, 125.8, 121.1, 120.1, 119.8, 117.5, 111.1, 110.9, 100.2, 28.2 ppm. HRMS (MALDI): calcd for $\text{C}_{35}\text{H}_{25}\text{F}_2\text{IrN}_2\text{O}_2$ 736.1513; found $[\text{M}^+] m/z$ 736.1510.

Complex 4d. Red solid (63%, 87 mg). ¹H NMR (400 MHz, CDCl_3) δ : 8.59 (d, J = 7.7, 2H), 8.01 (s, 2H), 7.90–7.80 (m, 4H), 7.70–7.55 (m, 10H), 7.46–7.40 (m, 4H), 6.95–6.91 (m, 2H), 6.67–6.61 (m, 4H), 4.71 (s, 1H), 1.55 (s, 6H) ppm. ¹³C-NMR (100 MHz, CDCl_3) δ : 185.6, 169.7, 150.8, 149.6, 147.2, 138.0, 136.2, 130.2, 129.8, 128.7, 127.1, 126.0, 125.8, 120.9, 117.1,

28.3 ppm. HRMS (MALDI): calcd for $\text{C}_{47}\text{H}_{35}\text{IrN}_2\text{O}_2$ 852.2328; found $[\text{M}^+] m/z$ 852.2329.

Complex 4e. Red solid (50%, 70 mg). ¹H NMR (400 MHz, CDCl_3) δ : 8.51 (d, J = 9.3 Hz, 2H), 7.69–7.65 (m, 2H), 7.62–7.59 (m, 4H), 7.49 (d, J = 7.6 Hz, 2H), 7.47 (d, J = 2.3 Hz, 2H), 7.40 (dd, J = 9.3, 2.4 Hz, 2H), 7.35–7.33 (m, 2H), 6.64 (t, J = 7.8 Hz, 2H), 6.34 (d, J = 7.9 Hz, 2H), 6.07 (d, J = 7.5 Hz, 2H), 5.27 (d, J = 14.6 Hz, 2H), 5.18 (d, J = 14.6 Hz, 2H), 4.96 (s, 1H), 1.73 (s, 6H) ppm. ¹³C-NMR (100 MHz, CDCl_3) δ : 186.1, 157.8, 149.5, 147.3, 144.2, 133.6, 133.1, 132.2, 131.6, 131.0, 129.4, 129.3, 129.2, 128.5, 128.4, 127.3, 125.6, 123.1, 107.8, 101.4, 66.2, 28.7 ppm. HRMS (MALDI): calcd for $\text{C}_{49}\text{H}_{33}\text{Cl}_2\text{IrN}_2\text{O}_4$ 976.1447; found $[\text{M}^+] m/z$ 976.1444.

Complex 4f. Red solid (67%, 118 mg). ¹H-NMR (400 MHz, CDCl_3) δ : 8.72 (d, J = 8.7 Hz, 2H), 8.59 (s, 2H), 8.31 (d, J = 9.0 Hz, 2H), 7.76–7.71 (m, 4H), 7.69–7.63 (m, 6H), 7.62–7.56 (m, 4H), 7.52–7.47 (m, 2H), 7.32–7.27 (m, 2H), 7.21 (dd, J = 9.1, 2.0 Hz, 2H), 7.03 (d, J = 8.4 Hz, 2H), 6.86 (d, J = 8.4 Hz, 2H), 4.65 (s, 1H), 2.41 (s, 6H), 1.51 (s, 6H) ppm. ¹³C-NMR (100 MHz, CDCl_3) δ : 185.4, 170.0, 157.9, 148.6, 148.5, 140.7, 138.6, 135.5, 135.4, 132.5, 132.0, 131.3, 129.8, 128.8, 128.6, 128.2, 126.5, 126.3, 124.9, 124.7, 122.3, 121.3, 121.3, 28.1, 21.5 ppm. HRMS (MALDI-TOF): calcd for $\text{C}_{57}\text{H}_{43}\text{IrN}_2\text{O}_2 \cdot \text{H}$ 981.3032; found $[\text{M} + \text{H}]^+ m/z$ 981.3029, $[\text{M-acac}]^+ m/z$ 881.2509.

Complex 4g. Red solid (71%, 123.0 mg). ¹H NMR (400 MHz, CDCl_3) δ : 8.32 (d, J = 9.5 Hz, 2H), 7.92 (d, J = 8.8 Hz, 2H), 7.85 (d, J = 8.8 Hz, 2H), 7.72 (d, J = 7.8 Hz, 2H), 7.31–7.26 (m, 8H), 7.23 (d, J = 2.7 Hz, 2H), 7.21 (d, J = 2.7 Hz, 1H), 7.19–7.15 (m, 8H), 7.10–7.04 (m, 5H), 6.90 (t, J = 7.4 Hz, 2H), 6.62 (t, J = 7.4 Hz, 2H), 6.55 (dd, J = 7.7, 1.2 Hz, 2H), 4.74 (s, 1H), 1.48 (s, 6H) ppm. ¹³C-NMR (100 MHz, CDCl_3) δ : 185.7, 168.2, 147.2, 145.7, 145.3, 136.4, 135.9, 129.5, 128.2, 127.5, 126.8, 125.1, 125.1, 123.7, 120.8, 117.0, 116.8, 100.2, 28.3 ppm. HRMS (MALDI): calcd for $\text{C}_{59}\text{H}_{45}\text{IrN}_4\text{O}_2$ 1034.3172; found $[\text{M}^+] m/z$ 1034.3169.

Complex 4h. Red solid (72%, 118 mg). ¹H-NMR (400 MHz, CDCl_3) δ : 8.59 (d, J = 9.0 Hz, 2H), 8.34 (s, 2H), 8.22 (s, 2H), 7.77–7.71 (m, 7H), 7.69–7.64 (m, 6H), 7.62–7.57 (m, 2H), 7.22 (d, J = 2.0 Hz, 1H), 7.16–7.07 (m, 6H), 6.97 (s, 2H), 4.71 (s, 1H), 2.41 (s, 6H), 1.52 (s, 6H) ppm. ¹³C-NMR (100 MHz, CDCl_3) δ : 185.4, 167.9, 149.3, 148.3, 147.9, 141.9, 138.3, 136.3, 134.7, 133.2, 132.3, 129.9, 129.8, 128.8, 128.7, 127.6, 126.3, 126.2, 125.8, 125.0, 124.9, 122.6, 117.7, 100.2, 28.4, 21.5 ppm. HRMS (MALDI-TOF): calcd for $\text{C}_{57}\text{H}_{43}\text{IrN}_2\text{O}_2 \cdot \text{H}$ 981.3032; found $[\text{M} + \text{H}]^+ m/z$ 981.3030, $[\text{M-acac}]^+ m/z$ 881.2506.

Complex 4i. Red solid (73%, 121 mg). ¹H-NMR (400 MHz, CDCl_3) δ : 8.70 (dd, J = 9.7, 5.5 Hz, 2H), 8.37 (s, 2H), 8.29 (s, 2H), 7.76–7.73 (m, 6H), 7.70–7.66 (m, 4H), 7.64–7.59 (m, 2H), 7.55 (dd, J = 9.8, 2.9 Hz, 2H), 7.18–7.13 (m, 8H), 6.95 (s, 2H), 4.72 (s, 1H), 1.53 (s, 6H) ppm. ¹³C-NMR (100 MHz, CDCl_3) δ : 185.6, 168.4, 149.4, 147.5, 146.7, 141.4, 137.5, 134.8, 133.2, 130.5, 130.5, 130.0, 129.6, 129.2, 129.0, 128.8, 127.3, 127.2, 126.6, 125.8, 125.5, 122.9, 120.0, 119.7, 118.3, 109.9, 109.7, 100.3, 28.4 ppm. HRMS (MALDI-TOF): calcd for $\text{C}_{55}\text{H}_{37}\text{F}_2\text{IrN}_2\text{O}_2$ 988.2452; found $[\text{M}^+] m/z$ 988.2451, $[\text{M-acac}]^+ m/z$ 889.2002.

Conflicts of interest

There are no conflicts to declare.

Acknowledgements

We thank the Colombian Institute for Science and Research (COLCIENCIAS) under the project No. RC-007-2017, Cod. 110274558597, for their financial support. CAEG acknowledges the postdoctoral program VIEF-UIS- Conv. 2018. CEPG acknowledges the fellowship given by the doctoral program COLCIENCIAS-Conv. 617. CHB acknowledges the use of research cyberinfrastructure resources and services provided by the Partnership for an Advanced Computing Environment (PACE) at the Georgia Institute of Technology. This research was supported in part through the computational resources and staff contributions provided for the Quest high performance computing facility at Northwestern University which is jointly supported by the Office of the Provost, the Office for Research, and Northwestern University Information Technology.

References

- B. O'regan and M. Grätzel, *Nature*, 1991, **353**, 737.
- A. Hagfeldt, G. Boschloo, L. Sun, L. Kloo and H. Pettersson, *Chem. Rev.*, 2010, **110**, 6595–6663.
- A. Harriman and J.-P. Sauvage, *Chem. Soc. Rev.*, 1996, **25**, 41–48.
- E. Baranoff, J.-P. Collin, L. Flamigni and J.-P. Sauvage, *Chem. Soc. Rev.*, 2004, **33**, 147–155.
- Y. H. Lee, O. Y. Kweon, H. Kim, J. H. Yoo, S. G. Han and J. H. Oh, *J. Mater. Chem. C*, 2018, **6**, 8569–8612.
- H. Zhu, J. Fan, B. Wang and X. Peng, *Chem. Soc. Rev.*, 2015, **44**, 4337–4366.
- A. N. Woodward, J. M. Kolesar, S. R. Hall, N.-A. Saleh, D. S. Jones and M. G. Walter, *J. Am. Chem. Soc.*, 2017, **139**, 8467–8473.
- X. Yang, G. Zhou and W.-Y. Wong, *Chem. Soc. Rev.*, 2015, **44**, 8484–8575.
- J. Liu, Y. Liu, Q. Liu, C. Li, L. Sun and F. Li, *J. Am. Chem. Soc.*, 2011, **133**, 15276–15279.
- Z. Mao, M. Wang, J. Liu, L.-J. Liu, S. M.-Y. Lee, C.-H. Leung and D.-L. Ma, *Chem. Commun.*, 2016, **52**, 4450–4453.
- Z. Yang, C. Huang, C. Wang, Y. Zhao and Q. Song, *ACS Sustainable Chem. Eng.*, 2017, **5**, 4443–4448.
- F. Maasoumi, R. D. Jansen-van Vuuren, P. E. Shaw, E. V. Puttock, R. C. R. Nagiri, J. A. McEwan, M. Bown, J. L. O'Connell, C. J. Dunn, P. L. Burn, *et al.*, *npj Flex. Electron.*, 2018, **2**, 27–32.
- G. Li, P. Li, X. Zhuang, K. Ye, Y. Liu and Y. Wang, *ACS Appl. Mater. Interfaces*, 2017, **9**, 11749–11758.
- B. Jiang, X. Ning, S. Gong, N. Jiang, C. Zhong, Z.-H. Lu and C. Yang, *J. Mater. Chem. C*, 2017, **5**, 10220–10224.
- S. Ladouceur, D. Fortin and E. Zysman-Colman, *Inorg. Chem.*, 2010, **49**, 5625–5641.
- S. Ladouceur, D. Fortin and E. Zysman-Colman, *Inorg. Chem.*, 2011, **50**, 11514–11526.
- K. K.-W. Lo, *Acc. Chem. Res.*, 2015, **48**, 2985–2995.
- E. Baranoff, J.-H. Yum, I. Jung, R. Vulcano, M. Grätzel and M. K. Nazeeruddin, *Chem. – Asian J.*, 2010, **5**, 496–499.
- Y.-J. Yuan, J.-Y. Zhang, Z.-T. Yu, J.-Y. Feng, W.-J. Luo, J.-H. Ye and Z.-G. Zou, *Inorg. Chem.*, 2012, **51**, 4123–4133.
- A. Kapturkiewicz, *Anal. Bioanal. Chem.*, 2016, **408**, 7013–7033.
- S. Ladouceur and E. Zysman-Colman, *Eur. J. Inorg. Chem.*, 2013, **2013**, 2985–3007.
- M. A. Baldo, M. E. Thompson and S. R. Forrest, *Nature*, 2000, **403**, 750–753.
- D.-L. Ma, C. Wu, W. Tang, A.-R. Gupta, F.-W. Lee, G. Li and C.-H. Leung, *J. Mater. Chem. B*, 2018, **6**, 537–544.
- Y. You and S. Y. Park, *Dalton Trans.*, 2009, 1267–1282.
- Q. Zhao, C.-Y. Jiang, M. Shi, F.-Y. Li, T. Yi, Y. Cao and C.-H. Huang, *Organometallics*, 2006, **25**, 3631–3638.
- L. Chen, S. Wang, Z. Yan, J. Ding and L. Wang, *J. Mater. Chem. C*, 2017, **5**, 5749–5756.
- H. U. Kim, J.-H. Jang, W. Song, B. J. Jung, J. Y. Lee and D.-H. Hwang, *J. Mater. Chem. C*, 2015, **3**, 12107–12115.
- X. Shang, D. Han, L. Zhao, L. Li and S. Lv, *Photochem. Photobiol. Sci.*, 2019, **18**, 1075–1080.
- N. Su, G.-Z. Lu and Y.-X. Zheng, *J. Mater. Chem. C*, 2018, **6**, 5778–5784.
- Z.-P. Yan, K. Liao, H.-B. Han, J. Su, Y.-X. Zheng and J.-L. Zuo, *Chem. Commun.*, 2019, **55**, 8215–8218.
- C. O. Kappe, *Angew. Chem., Int. Ed.*, 2004, **43**, 6250–6284.
- M. B. Gawande, S. N. Shelke, R. Zboril and R. S. Varma, *Acc. Chem. Res.*, 2014, **47**, 1338–1348.
- K. Saito, N. Matsusue, H. Kanno, Y. Hamada, H. Takahashi and T. Matsumura, *Jpn. J. Appl. Phys.*, 2004, **43**, 2733–2734.
- N. Yoshikawa and T. Matsumura-Inoue, *Anal. Sci.*, 2003, **19**, 761–765.
- T. M. Monos, A. C. Sun, R. C. McAtee, J. J. Devery III and C. R. J. Stephenson, *J. Org. Chem.*, 2016, **81**, 6988–6994.
- M. Nonoyama, *Bull. Chem. Soc. Jpn.*, 1974, **47**, 767–768.
- J. Zhou, W. Xu, Z. You, Z. Wang, Y. Luo, L. Gao, C. Yin, R. Peng and L. Lan, *Sci. Rep.*, 2016, **6**, 25149–25154.
- B. Orwat, E. Witkowska, I. Kownacki, M.-J. Oh, M. Hoffmann, M. Kubicki, I. Grzelak, B. Marciniak, I. Glowacki, B. Luszczynska, *et al.*, *Dalton Trans.*, 2017, **46**, 9210–9226.
- Y. Li, Y. Liu and M. Zhou, *Dalton Trans.*, 2012, **41**, 3807–3816.
- Y.-H. Chang, K. Takeuchi, M. Wakioka and F. Ozawa, *Organometallics*, 2015, **34**, 1957–1962.
- A. P. Wilde and R. J. Watts, *J. Phys. Chem.*, 1991, **95**, 622–629.
- C. Yang, F. Mehmood, T. L. Lam, S. L.-F. Chan, Y. Wu, C.-S. Yeung, X. Guan, K. Li, C. Y.-S. Chung, C.-Y. Zhou, *et al.*, *Chem. Sci.*, 2016, **7**, 3123–3136.

- 43 M. Bixon, J. Jortner, J. Cortes, H. Heitele and M. E. Michel-Beyerle, *J. Phys. Chem.*, 1994, **98**, 7289–7299.
- 44 F.-I. Wu, H.-J. Su, C.-F. Shu, L. Luo, W.-G. Diao, C.-H. Cheng, J.-P. Duan and G.-H. Lee, *J. Mater. Chem.*, 2005, **15**, 1035–1042.
- 45 E. Baranoff, I. M. Dixon, J.-P. Collin, J.-P. Sauvage, B. Ventura and L. Flamigni, *Inorg. Chem.*, 2004, **43**, 3057–3066.
- 46 E. Baranoff and P. Kumar, *Iridium Optoelectron. Photonics Appl.*, 2017, 655–681.
- 47 P. Duan, N. Yanai and N. Kimizuka, *Chem. Commun.*, 2014, **50**, 13111–13113.
- 48 M. Valiev, E. J. Bylaska, N. Govind, K. Kowalski, T. P. Straatsma, H. J. J. Van Dam, D. Wang, J. Nieplocha, E. Apra, T. L. Windus, *et al.*, *Comput. Phys. Commun.*, 2010, **181**, 1477–1489.